Available online at www.sciencedirect.com
SCIENCE DIRECT®
Biomaterials 27 (2006) 2150–2161
Biomaterials
www.elsevier.com/locate/biomaterials

# A computer modelling study of the uptake, structure and distribution of carbonate defects in hydroxy-apatite

Sherina Peroos[a], Zhimei Du[b], Nora Henriette de Leeuw[a,b,*]

[a]*Department of Chemistry, University College London, 20 Gordon Street, London WC1 H 0AJ, UK*
[b]*School of Crystallography, Birkbeck College London, Malet Street, London WC1E 7HX, UK*

Received 23 May 2005; accepted 26 September 2005
Available online 11 October 2005

**Abstract**

Computer modelling techniques have been employed to qualitatively and quantitatively investigate the uptake and distribution of carbonate groups in the hydroxyapatite lattice. Two substitutional defects are considered: the type-A defect, where the carbonate group is located in the hydroxy channel, and the type-B defect, where the carbonate group is located at the position of a phosphate group. A combined type A–B defect is also considered and different charge compensations have been taken into account. The lowest energy configuration of the A-type carbonate has the O–C–O axis aligned with the channel in the *c*-direction of the apatite lattice and the third oxygen atom lying in the *a*/*b* plane. The orientation of the carbonate of the B-type defect is strongly affected by the composition of the apatite material, varying from a position (almost) flat in the *a*/*b* plane to being orientated with its plane in the *b*/*c* plane. However, Ca–O interactions are always maximised and charge compensating ions are located near the carbonate ion.

When we make a direct comparison of the energies per substitutional carbonate group, the results of the different defect simulations show that the type-A defect where two hydroxy groups are replaced by one carbonate group is energetically preferred ($\Delta H = -404\,\mathrm{kJ\,mol^{-1}}$), followed by the combined A–B defect, where both a phosphate and a hydroxy group are replaced by two carbonate groups ($\Delta H = -259\,\mathrm{kJ\,mol^{-1}}$). The type-B defect, where we have replaced a phosphate group by both a carbonate group and another hydroxy group in the same location is energetically neutral ($\Delta H = -1\,\mathrm{kJ\,mol^{-1}}$), but when the replacement of the phosphate group by a carbonate is charge compensated by the substitution of a sodium or potassium ion for a calcium ion, the resulting type-B defect is energetically favourable ($\Delta H_{\mathrm{Na}} = -71\,\mathrm{kJ\,mol^{-1}}, \Delta H_{\mathrm{K}} = -6\,\mathrm{kJ\,mol^{-1}}$) and its formation is also promoted by A-type defects present in the lattice. Our simulations suggest that it is energetically possible for all substitutions to occur, which are calculated as ion-exchange reactions from aqueous solution. Carbonate defects are widely found in biological hydroxy-apatite and our simulations, showing that incorporation of carbonate from solution into the hydroxyapatite lattice is thermodynamically feasible, hence agree with experiment.


*Keywords:* Hydroxyapatite; Apatite structure; Calcium carbonate; Molecular modelling; Carbonate defects

## 1. Introduction

Apatites $Ca_{10}(PO_4)_6(F,Cl,OH)_2$ are a complex and diverse class of materials, which are becoming increasingly important as candidates for use as bio-materials. In the geological environment, they are the most abundant phosphorus-bearing minerals, found extensively in igneous, metamorphic and sedimentary rocks [1]. More recently, however, they have gained additional prominence due to their biological role as one of the main constituents of mammalian bones and tooth enamel [2]. The presence of hydroxyapatite in bone and tooth enamel gives rise to its utility in a range of biomedical applications, for example, in the manufacture of artificial bone material and as a coating on surgical implants. Research has shown that polycrystalline calcium phosphate can directly bond to bone, which is regarded as the precursor to bone apatite

*Corresponding author. Department of Chemistry, University College London, 20 Gordon Street, London WC1 H 0AJ, UK. Tel.: +44 20 7679 1015; fax: +44 20 7679 7463.
*E-mail address:* n.h.deleeuw@ucl.ac.uk (N.H. de Leeuw).

0142-9612/$ - see front matter © 2005 Elsevier Ltd. All rights reserved.
doi:10.1016/j.biomaterials.2005.09.025

formation in vivo [3]. The good biocompatibility of these calcium phosphates indicates their suitability in repair or replacement of damaged or diseased bone. To improve the strength of the relatively brittle hydroxyapatite, a metallic implant can be coated with hydroxyapatite, which will encourage bonding with the living bone, aiding the acceptance of the implant material by the body [4,5].

Natural bone also contains an appreciable proportion of calcite $CaCO_3$ [2], and carbonate defects are therefore an important consideration in biological hydroxyapatite. Apatites with up to 5–6% $CO_3^{2-}$ and less than 1% fluoride are often referred to as dahllite and due to the appreciable content of carbonate rather than fluoride in bone and tooth enamel, the apatite mineral present in bone is therefore sometimes also referred to as dahllite. In dental enamel, the hydroxyapatite crystals are found as prisms or rods made up of dense hydroxyapatite clusters of dimensions relatively bigger than those in bone [2], with appreciable amounts of fluoride, magnesium and carbonate impurities. The presence of these carbonate impurities in hydroxyapatite alters the physical and chemical properties of the material and it has been shown that a higher carbonate content is associated with a smaller grain size, a reduction in crystallinity and an increase in the extent of dissolution of apatites [5–9].

Local structural details of apatite have still not been resolved in detail as intact bone is a demanding material for structural studies, due to its ''morphological diversity, the coexistence, interrelationship and great complexity of its organic and inorganic components and the substantial sensitivity of bone samples to physical and chemical effects'' [6,7]. However, a large range of structure determination methods has been employed to analyse the structure of biological and synthetic hydroxyapatite and the locations of carbonate defects within them [10–12]. Substitutional $CO_3^{2-}$ defects are labeled as A- and B-type defects, depending on whether they occupy the $OH^-$ or $PO_4^{3-}$ sites in the hydroxyapatite structure, respectively [13–16]. Studies on tooth enamel and apatites synthesized at high temperatures identified carbonate groups located in the hydroxy channels, replacing the hydroxy ions, leading to an increase in the *a*-parameter of the apatite lattice [6,13]. Substitutional carbonate groups in phosphate locations were observed in human bone mineral [18] and again in high-temperature synthetic apatites [18–21], which was accompanied by a shrinkage in the *a*-parameter of the lattice due to its smaller size [11,22,28]. Many structural determinations of hydroxyapatite have in fact observed a mixture of these two carbonate defects within the same lattice [7,13,23,24], as well as a mixture of carbonate and other defects, for example $HPO_4^{2-}$ species [5,9,25], $OH^-$ deficiency [5] and a low calcium content [25,26].

The present study reports a detailed, atomic-level computational study of the uptake of carbonate groups from solution into the hydroxyapatite crystal, replacing either phosphate or hydroxy groups in the lattice. Computational methods are well placed to calculate at the atomic level the energetics of carbonate uptake and distribution in the hydroxyapatite material and our approach is to employ interatomic potential methods, as these methods combine the accuracy required to investigate the defect structures and to calculate the energetics of the exchange reactions with the computational efficiency to sample the necessarily large numbers of different defect configurations to obtain the thermodynamically preferred structures for direct comparison.

## 2. Theoretical methods

The perfect and defective apatite lattices were modelled using interatomic potential-based simulation techniques, based on the Born model of solids [27], which assumes that the ions in the crystal interact via long-range electrostatic forces and short-range forces, including both the repulsions and van der Waals attractions between neighbouring electron charge clouds, which are described by simple parameterised analytical functions. The electronic polarisability is included via the shell model of Dick and Overhauser [28], where each polarisable ion, in our case the oxygen ion, is represented by a core and a massless shell, connected by a spring. The polarisability of the model ion is then determined by the spring constant and the charges of the core and shell. When necessary, angle-dependent forces are included to allow directionality of bonding as for example, in the covalent phosphate and carbonate anions. We have employed the energy minimisation code METADISE [29] to calculate the various carbonate defects in the hydroxyapatite lattice in a three-dimensional periodic boundary approach, at all times ensuring that sufficiently large supercells are employed to avoid finite size effects and interactions between the repeating images. METADISE has been used successfully for a range of simulations of complex oxide materials, including surface adsorption [30] and reconstruction simulations [31] and bulk defect calculations [32,33].

We have used molecular dynamics (MD) simulations for the calculation of the energies of the hydrated ions, which were necessary to calculate the ion-exchange reactions. In addition, we have investigated the most stable A-type defect, i.e. where a carbonate replaces two hydroxy groups, with MD simulations to investigate whether the carbonate configuration is stationary in the apatite lattice, vibrating about its equilibrium position only, or whether it rotates/tumbles in its location. The MD code used was DL_POLY [34], where the integration algorithms are based around the Verlet leap-frog scheme [35]. We used the Nosé-Hoover algorithm for the thermostat [36,37], as this algorithm generates trajectories in both NVT and NPT ensembles, thus keeping our simulations consistent. The Nosé-Hoover parameters were set at 0.5 ps for both the thermostat and barostat relaxation times. The simulation temperature was set at 310 K, which fluctuated by less than 10 K during the data collection run of 200 ps duration with a timestep of 0.2 fs.

### 2.1. Potential model

In recent publications, we have empirically derived interatomic potential parameters for the simulation of the hydroxyapatite material [30,33], which were also tested against electronic structure calculations, and shown to give excellent agreement with experimental fluor- and hydroxyapatite structures and properties. As carbonate impurities in the apatite material were always an important consideration, even at the stage of first deriving the fluor- and hydroxy-apatite interatomic potential parameters, the apatite potential models were fitted to be compatible with existing calcium carbonate potential models [38], which have been used successfully in a range of simulations of bulk and surface properties [38,39], defect and sorption calculations [40,41]. In this study we have therefore employed the combined calcium carbonate/hydroxy-apatite potential model, listed in Table 1, to calculate the structures and energies of the different A- and B-type carbonate defects in the hydroxyapatite lattice. The potential parameters for the sodium and potassium ions, which were used to charge compensate certain of the B-

Table 1
Potential parameters (short-range cutoff 20 Å, short-range parameters between shells unless stated otherwise)

| Ion | Charges (e) | | |
|---|---|---|---|
| | Core | Shell | Core-shell interaction (eV Å$^{-2}$) |
| Ca | +2.000 | | |
| Na | +1.000 | | |
| K | +1.000 | | |
| P | +1.180 | | |
| H | +0.400 | | |
| C | +1.135 | | |
| Phosphate/carbonate oxygen (O) | +0.587 | −1.632 | 507.4000 |
| Hydroxy oxygen (Oh) | +0.900 | −2.300 | 74.92038 |
| *Buckingham potential* | | | |
| Ion pair | $A$ (eV) | $\rho$ (Å) | $C$ (eVÅ$^6$) |
| Ca–O | 1550.0 | 0.297 | 0.0 |
| Ca–Oh | 1250.0 | 0.344 | 0.0 |
| C–Oh | 709.4 | 0.344 | 0.0 |
| Na–O | 661.3 | 0.3065 | 0.0 |
| Na–Oh | 886.8 | 0.3065 | 0.0 |
| K–O | 355.5 | 0.3798 | 0.0 |
| K–Oh | 476.3 | 0.3798 | 0.0 |
| H–O | 312.0 | 0.250 | 0.0 |
| H–Oh | 312.0 | 0.250 | 0.0 |
| O–O | 16372.0 | 0.213 | 3.47 |
| Oh–Oh | 22764.0 | 0.149 | 6.97 |
| O–Oh | 22764.0 | 0.149 | 4.92 |
| *Morse potential* | | | |
| | $D$ (eV) | $\alpha$ (Å$^{-1}$) | $r_0$ (Å) |
| P–$O_{core}$ | 3.47 | 1.900 | 1.600 |
| C–$O_{core}$ | 4.71 | 3.800 | 1.180 |
| H–Oh | 7.0525 | 3.1749 | 0.9485 |
| *Three-body potential* | | | |
| | $k$ (eV rad$^{-2}$) | $\Theta_0$ | |
| $O_{core}$—P–$O_{core}$ | 1.322626 | 109.47 | |
| $O_{core}$—C–$O_{core}$ | 1.690 | 120.0 | |
| *Four-body potential* | | | |
| | $k$ (eV rad$^{-2}$) | $\Theta_0$ | |
| $O_{core}$–C–$O_{core}$ | 0.1129 | 180.0 | |
| *Intramolecular coulombic interaction (%)* | | | |
| H–Oh | 0 | | |

type defect structures, were taken from the work by Purton et al. [42] and scaled to allow for the partial charges of the oxygen atoms, following the well-proven method by Schroeder et al. [43] and finally tested against the structure of $Na_3PO_4$.

## 3. Results and discussion

Biological apatite material has a hexagonal crystal structure with spacegroup $P6_3/m$, $a = b = 9.36-9.64$ Å, $c = 6.78-6.90$ Å, $\alpha = \beta = 90^\circ$, $\gamma = 120^\circ$ [1,2], which upon geometry optimisation relaxed to $a = b = 9.34$ Å, $c = 6.87$ Å, $\alpha = \beta = 90^\circ$, $\gamma = 120^\circ$ for the hydroxyapatite end-member. The hydroxy groups in the apatite structure are all stacked above each other in hexagonal channels in the $c$-direction, where each $OH^-$ is coordinated to three surrounding Ca ions which lie in the same $a/b$ plane, shown in Fig. 1. Alternate rotation of the Ca positions in the $a/b$-plane gives rise to the hexagonally shaped channels. In the ideal structure, the OH groups are stacked in a regular column within the channels, although the direction of the OH groups in the columns may differ randomly between neighbouring channels [44,45]. However, as synthetic hydroxy apatite crystallises in a fully ordered monoclinic structure with spacegroup $P2_1/b$, which structure is in effect a doubling of the hexagonal unit cell, but with all possible OH positions defined, we have used the monoclinic cell for our simulations, when necessary using $2 \times 1$ and $2 \times 2$ supercells. Once the simulation cell is created, it is essentially a P1 structure, as no symmetry constraints are used in the simulations and all species in the simulation cell are free to move independently from one another. In addition, the simulation cell itself is allowed to contract/expand and deform anisotropically.

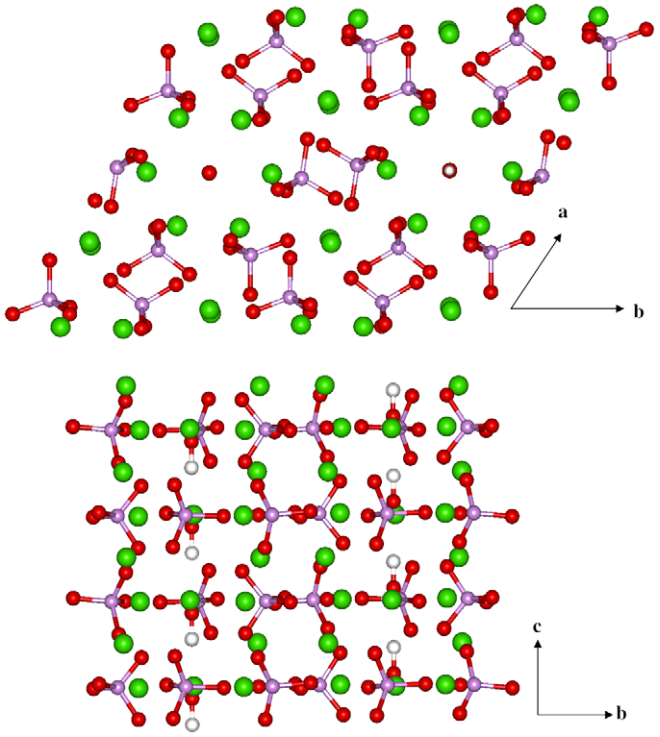


Fig. 1. Plan and side views of the hydroxyapatite structure, showing the $OH^-$ groups in hexagonal channels surrounded by Ca ions (O = red, Ca = green, P = pink, H = white).

Full information of the cell parameters and atomic coordinates of all minimum energy defect structures is available from the corresponding author.

### 3.1. Type-A defect

We first investigated the type-A defect, where carbonate groups are located in the hydroxy channel. For each carbonate group incorporated into the lattice, two hydroxy groups were deleted for charge compensation (and also steric hindrance, which might otherwise occur in the hydroxy channel), as shown in Eq. (1). A range of different starting configurations of the carbonate ion was studied, including in an upright position at different rotations in the $a/b$-plane and lying flat in the $a/b$-plane, but rotated about the $c$-axis at various angles. In addition to different initial configurations of the carbonate group itself, a number of different locations of the carbonate ion in the hydroxy channel were also studied, i.e. locating the carbonate group at the $OH^-$ positions, as well as locating it midway between the two hydroxy vacancies. In addition to replacing two adjacent hydroxy groups by the carbonate group, we also investigated the replacement by the carbonate of two hydroxy groups, one in each of two neighbouring channels, but, as could be expected, this configuration where both channels had excess charge (+1 in the channel with the hydroxy vacancy and −1 in the channel with the replacement carbonate group) was not energetically very favourable, especially as the substitutional carbonate group had also less space in the single $OH^-$ vacancy than when it was located in a channel with two vacancies. This configuration was 131.8 kJ mol$^{-1}$ less favourable than the configurations with the carbonate replacing two hydroxy groups in the same channel.

$$Ca_{40}(PO_4)_{24}(OH)_8 + CO^{2-}_{3(aq)} \rightarrow Ca_{40}(PO_4)_{24}(CO_3)(OH)_6 + 2OH^-_{(aq)} \quad (1)$$

The most stable configuration of the carbonate group substituting for two hydroxy groups in the channel is shown in Fig. 2, where the carbonate is located almost midway between the two hydroxy vacancies with two oxygen ions more or less aligned in the $c$-direction and the central oxygen ion lying in the $a/b$-plane. The carbonate is located closer to the hydroxy group which has its hydrogen ion pointing towards the carbonate (shown at the bottom in Fig. 2), leading to fairly long hydrogen-bonded interactions between this hydroxy hydrogen and one of the carbonate oxygen ions ($O_2CO\cdots HO = 2.75$ Å). The carbonate group is repelled by the other neighbouring hydroxy group, which has its oxygen directed towards

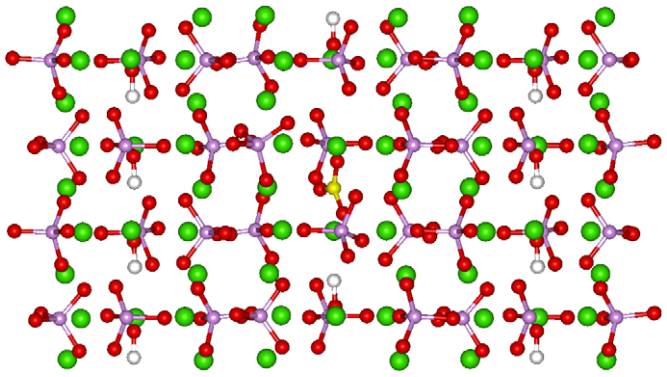

Fig. 2. Side view of the lowest energy monoclinic hydroxyapatite structure with A-type carbonate defect (O = red, Ca = green, P = pink, H = white, C = yellow).

another oxygen atom of the carbonate group ($HO\cdots OCO_2 = 4.72$ Å). Other interactions between the substitutional carbonate and the apatite lattice include those between its oxygen ions and lattice calcium ions (three interactions each for the top and bottom oxygen with surrounding calcium ions with $Ca\cdots OCO_2 = 2.24$–$3.13$ Å, in agreement with experiment [15], but no significant interactions between the central oxygen atom and surrounding calcium ions). However, the location of the carbonate along the channel can vary easily without significant energetic penalty. The difference in energy between the carbonate located in either hydroxy vacancy position or midway between the two vacancies is only about 2.9 kJ mol$^{-1}$ and all three positions are therefore about equally feasible. Peeters et al. [16] in their static lattice DFT study calculated that the planar $CO_3$ impurity in its most stable position lay oriented in a plane at an angle of 7° with the crystallographic *c*-axis, which is similar to the orientation of the carbonate ion in the hydroxy channel found in our simulations, which is also in agreement with the experimental structure elucidated by Fleet et al. [46,47], where the carbonate plane was tilted by approximately 12° with respect to the *c*-axis.

### 3.1.1. Molecular dynamics simulations

Our energy minimisation calculations showed that different orientations of the carbonate group in the channel do not lead to significantly different energies, with energy variations of up to 1 kJ mol$^{-1}$ only. To test whether the carbonate group is free to rotate in its position in the channel when temperature was taken into account, we carried out MD simulations of the system at 310 K. Fig. 3 shows a series of snapshots of the system taken at different times during the MD simulation, which clearly show that the carbonate group is not stationary in the lattice, but rotates around an axis in the *c*-direction of the apatite lattice (Fig. 3a–d), approximately the O–C–O alignment of the carbonate ion. This rotation, which is a smooth continuous movement, is probably due to the fact that, as we saw in Section 3.1 above, the central oxygen atom of the carbonate group is not interacting with lattice calcium atoms which interactions, if present, would hinder free rotation.

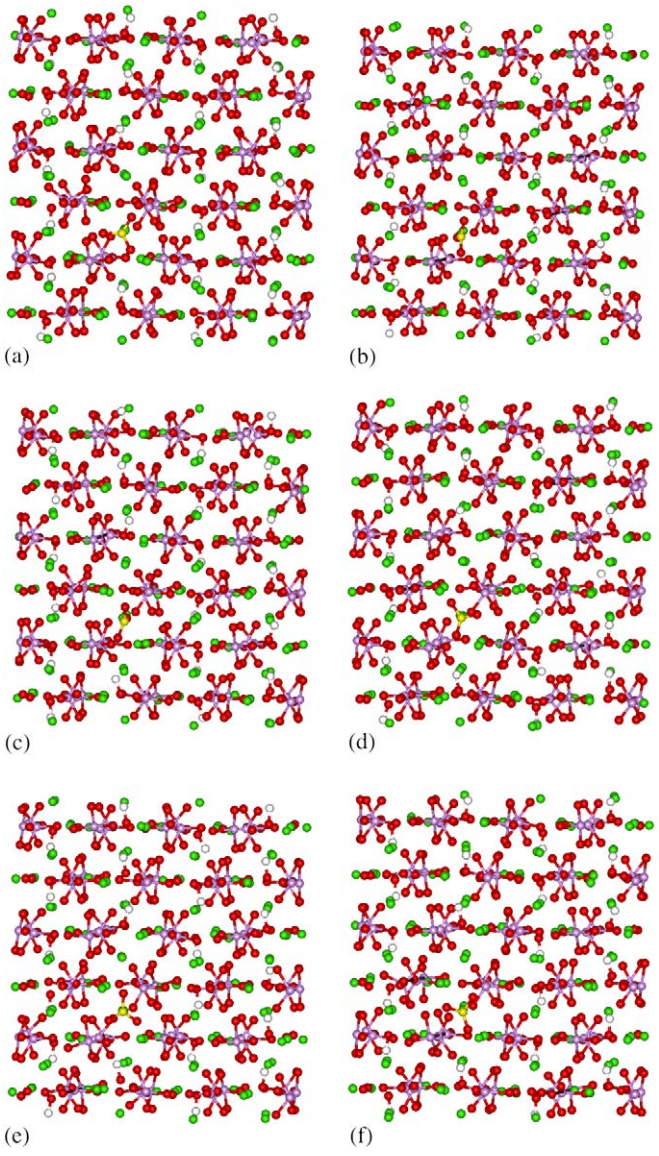


Fig. 3. Series of snapshots of molecular dynamics simulations of the A-type defect, replacing two adjacent hydroxy groups in the channel by one carbonate, showing (a–d) free rotation of the carbonate around an axis in the *c*-direction and (e,f) tumbling along axes in the *a*/*b* plane (O = red, Ca = green, P = pink, H = white, C = yellow).

In addition, but less frequently, the whole carbonate molecule rotates about an axis through its carbon atom perpendicular to the plane of the molecule, with the effect that the oxygen atoms of the carbonate exchange positions (Fig. 3a, d–f). From the simulations we see that this rotation does not appear to be a smooth, incremental movement like the rotation of the central oxygen around the *c*-axis described above and shown in Figs. 3a–d, and the top and bottom oxygen positions are retained during most of the simulation apart from the occasional rapid exchange. This motion indicates that there is an energy

barrier associated with this exchange in O positions, which, however, can be overcome at this temperature. The carbonate group resides most of the time in one of several minimum energy configurations, but occasionally the energy barrier is overcome sufficiently to rotate the group into the next low energy configuration.

Finally, there does not appear to be any movement of the carbonate group along the channel in the *c*-direction, even though the energies from the energy minimisation calculations change little with a shift up or down the channel. Presumably then, the lack of movement of the carbonate along the *c*-direction is due to an energy barrier, which is not overcome in these MD simulations at moderate temperature. The close interactions between the top and bottom oxygen atoms with three lattice calcium ions each would have to be broken and reformed when a shift occurs along the *c*-direction, which would lead to an intermediate high-energy configuration during the movement.

Both the energy minimisation and MD simulations thus indicate that the orientation of the carbonate group in the channel is preferentially with one oxygen at the top and one oxygen at the bottom in the channel, but that the third, central oxygen is mobile within the *a*/*b*-plane with rotation of this third oxygen around the O–C–O axis in the *c*-direction.

### 3.2. Type-B defect

In the type-B defect structure, the carbonate substitutes for a phosphate group in the apatite lattice. We have considered two types of B defects, firstly where the charge compensation is effected by the incorporation of an extra hydroxy group near the carbonate, in effect replacing a phosphate group by a carbonate and hydroxy group in the same location (Eq. (2)):

$$Ca_{20}(PO_4)_{12}(OH)_4 + CO^{2-}_{3(aq)} + OH^{-}_{(aq)} \rightarrow Ca_{20}(PO_4)_{11}(CO_3)(OH)_5 + PO^{3-}_{4(aq)} \quad (2)$$

and secondly, charge compensating the B-type defect by replacing a calcium ion by a monovalent Na or K ion (Eq. (3)):

$$Ca_{20}(PO_4)_{12}(OH)_4 + CO^{2-}_{3(aq)} + M^{+}_{(aq)} \rightarrow Ca_{19}M(PO_4)_{11}(CO_3)(OH)_4 + PO^{3-}_{4(aq)} + Ca^{2+}_{(aq)} \quad (3)$$

#### 3.2.1. Phosphate substitution by $CO_3^{2-}/OH^-$

There are three inequivalent phosphate groups in the monoclinic apatite unit cell and we have investigated substitutions of all three phosphate groups by the carbonate/hydroxy defect, as well as considering all different configurations of the carbonate within the phosphate vacancy, i.e. for each phosphate group we replaced the phosphorus atom by a carbonate and used three of the original phosphate oxygen positions for its oxygen atoms, and the fourth as the initial oxygen atom of the extra hydroxy group. We considered all possible permutations of the four oxygen positions for each replaced phosphate group and, in addition, considered a range of different starting positions for the hydrogen atom of the extra hydroxy group.

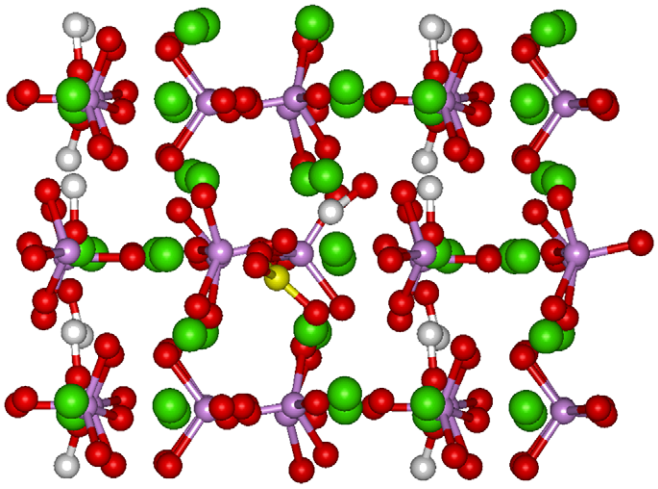

Fig. 4. Side view of the lowest energy hydroxyapatite structure with B-type carbonate defect, created by replacing a $PO_4^{3-}$ group by one $CO_3^{2-}$ and one $OH^-$ (O = red, Ca = green, P = pink, H = white, C = yellow).

The lowest energy configuration of this type-B defect is shown in Fig. 4, where we see that both the hydroxy group and to a lesser extend the carbonate group have moved away from the phosphate position. There is no clear energetic preference by the carbonate and hydroxy group to substitute for any particular phosphate group, as the defect energies for all three inequivalent phosphate locations are all within about 10 kJ mol$^{-1}$ of each other. In addition, the defect energies for all the different orientations of the carbonate group within the phosphate positions are also very similar ($\Delta E < 5$ kJ mol$^{-1}$). After geometry optimisation of each particular starting configuration, the final structure always shows the hydrogen of the hydroxy group pointing towards the carbonate group, forming hydrogen-bonded interactions with two of its oxygen atoms, where the H$\cdots$O bond distances range from 2.15 to 2.41 Å. This orientation, which is probably one of the reasons why the carbonate and hydroxy groups have moved away from the phosphate position, also maximises O–Ca interactions between the hydroxy oxygen atom and lattice calcium ions, with O–Ca distances starting from 2.20 Å.

The least stable structures, with defect energies higher by up to 100 kJ mol$^{-1}$, are those where the hydroxy ion and carbonate group are even further apart than in Fig. 4, which added instability is probably due to a combination of charge separation of the defects, together with a loss of the hydrogen-bonding interactions between them, rather than steric effects, as separation of the two substitutional groups leads to less crowding of the phosphate vacancy location.

### 3.2.2. Phosphate substitution by $CO_3^{2-}/M^+$

In the second type-B defect structure we studied, one of the calcium ions near the substitutional carbonate group is replaced by either a sodium or potassium ion. The defect site is hence partially vacant as only three of the four phosphate oxygen atoms are used in the carbonate group. As in the previous simulations, we considered all possible orientations of the carbonate group in the three phosphate positions as starting structures, and we also considered all possible permutations of replaced calcium ions for each carbonate location and orientation. Similar to the $CO_3^{2-}/OH^-$ type-B defect described above, the lowest energy defect structures are those where the substitutional carbonate group and monovalent cation were located closely together, becoming less stable as their separation within the simulation cell increases.

Fig. 5 shows the lowest energy structure of the B-type defect with a $K^+$ ion replacing one of the calcium ions. As might have been expected, the geometry optimised structures for either $Na^+$ and $K^+$ ions charge balancing for the substitutional carbonate defect are so similar (although the energies are not), that we have not shown the $Na^+$ system as well. In the lowest energy structures, the carbonate group is lying almost flat in the $a/b$-plane of the apatite lattice, in agreement with experimental structures of B-type carbonate defects charge balanced by $Ca^{2+}$ vacancies, elucidated from FT-IR measurements ([14] and references therein), and X-ray powder diffraction studies [48]. However, the molecule does not lie completely flat in the $a/b$ plane, but the normal to the plane of the carbonate molecule is tilted at a small angle of approximately 15° to the $c$-axis of the lattice, which is in reasonable agreement with recent Rietveld structure refinements of B-type $CO_3$ defects in sodium containing apatites, where an angle of approximately 30° with the $c$-axis was found [49]. However, in the least stable structures, when the sodium or potassium ion is located at a position farther away, i.e. an ordinary $Ca^{2+}$ is located near the carbonate defect, the plane of the carbonate group is more or less orientated in the $b/c$-plane. It thus appears that the orientation of the B-type carbonate defect is very dependent on the type and location of the charge compensating ions present in the lattice. Note, however, that the energy differences between highest and lowest energy structures are again very small ($\Delta E < 2\,kJ\,mol^{-1}$) and there is thus no clearly preferred candidate amongst the range of final geometry optimised structures. The carbonate group is now located in the phosphate lattice position, rather than just off it as in the $CO_3/OH$ defect described above, which displacement was due to the extra hydroxy group near the carbonate defect. The calcium ion that is preferentially replaced by the $Na^+$ ion is at a distance of approximately 3.11–4.02 Å from the oxygen ions of the carbonate group, although the correlation between the relative positions of the $K^+$ ion and the carbonate group is not as clear. The detailed calculations of the relative stabilities of the different types of defects and the energetics of their uptake from solution are discussed in Section 3.5 below, but suffice it to say here that the process of replacing calcium ions by $Na^+$ is energetically more favourable than using $K^+$ as a charge balancing cation. This difference in defect energies may be explained by the ionic radii of the three cations, which are listed in Table 2 [50]. The ionic radii of $Ca^{2+}$ and $Na^+$ are very similar, whereas the ionic radius of $K^+$ is significantly larger. Based on the argument that the uptake of impurity ions in a crystal lattice is governed by the elastic strain and that smaller ions thus can be more easily incorporated than bigger impurity ions, the incorporation of the bigger potassium ion at a calcium site should be more difficult than the incorporation of sodium, which is indeed what we observe.

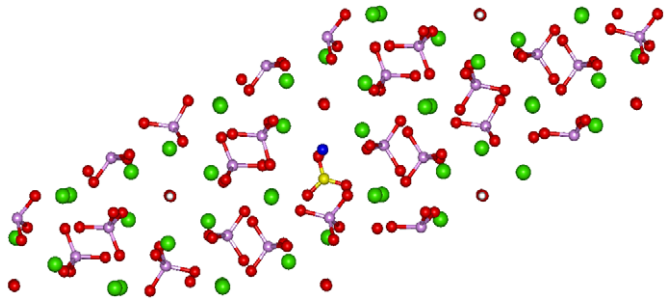

Fig. 5. Plan of the lowest energy hydroxyapatite structure with B-type carbonate defect, created by replacing a $PO_4^{3-}$ group by a $CO_3^{2-}$ group and one $Ca^{2+}$ ion by a $K^+$ ion (O = red, Ca = green, K = blue, P = pink, H = white, C = yellow).

### 3.3. Type-A/B defect

In addition to separate simulations of the type-A and -B defects in the apatite lattice, we have also investigated the defect structures and energies of a combination of the two defects, where we replace one phosphate group and one channel hydroxy group by a carbonate group each (Eq. (4)). Many experimental studies have observed carbonates in both the hydroxy and the phosphate sites within the same lattice [6–8,13,23,24] and we thus need to take this combination into account.

$$Ca_{20}(PO_4)_{12}(OH)_4 + 2CO_{3(aq)}^{2-} \rightarrow Ca_{20}(PO_4)_{11}(CO_3)_2(OH)_3 + OH_{(aq)}^- + PO_{4(aq)}^{3-} \quad (4)$$

As before, we have considered all possible combinations and orientations of the carbonates in the phosphate locations and in the channel. Again, the energy differences

Table 2
Ionic radii

| Ion | Ionic radius (pm) |
|---|---|
| $Ca^{2+}$ | 100 |
| $Na^+$ | 102 |
| $K^+$ | 138 |

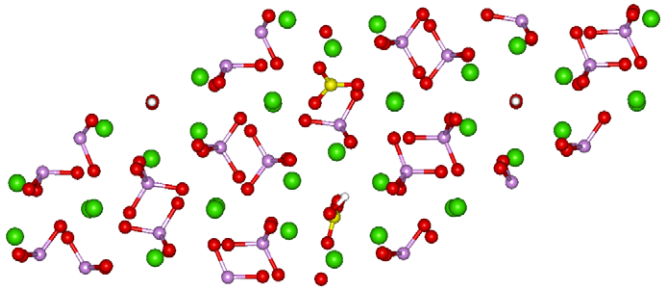

Fig. 6. Plan view of the lowest energy hydroxyapatite structure with combined A- and B-type carbonate defects, created by replacing one $PO_4^{3-}$ group and one $OH^-$ ion by two $CO_3^{2-}$ groups (O = red, Ca = green, P = pink, H = white, C = yellow).

Table 3
Percentage increase/decrease in lattice parameters due to carbonate defects for the lowest energy defect structures

| Lattice parameter | % Increase or decrease in calculated lattice parameters | | | | |
|---|---|---|---|---|---|
| | Type-A channel | Type-B $PO_4$ position | | | Type-A/B |
| | MD simulation | $CO_3$/OH | $CO_3$/Na | $CO_3$/K | Mixed |
| *a* | +0.02 | −0.75 | −0.39 | −0.30 | −0.93 |
| *b* | +0.02 | −0.27 | −0.48 | −0.37 | −0.70 |
| *c* | +0.01 | +0.75 | +0.07 | +0.14 | +0.86 |

between substitution of any of the three inequivalent phosphate groups were insignificant ($< 2\,kJ\,mol^{-1}$), but the lowest energy structure is shown in Fig. 6. The local structure of this mixed defect is slightly different from the isolated A- and B-type defects. The carbonate group that replaces the phosphate is again located almost in the phosphate lattice position, as was the case in the $CO_3$/M type-B defect structure described above, and in reasonable agreement with experimental findings [51]. However, the carbonate in the channel now replaces only one channel hydroxy group, leading to more crowding and although this carbonate group is still positioned almost upright in the channel, it is now at the OH lattice position, in agreement with single-crystal X-ray data of type-A/B defects [51]. However, the neighbouring hydroxy group has rotated in the channel, now lying almost flat in the *a*/*b* plane, thereby minimising any steric hindrance and maximising H-bonding interactions with carbonate oxygen atoms ($OH\cdots OCO_2 = 2.24$–$2.77$ Å).

### 3.4. Effect of carbonate defects on hydroxyapatite lattice parameters

Experimental studies have shown that the presence of carbonate defects in the hydroxyapatite lattice leads to changes in the lattice parameters. The incorporation of type-A carbonate defects in the channel causes an increase of the *a*-parameter [6.13], whereas the type-B substitution of a phosphate group by a carbonate leads to contraction of the *a*-axis [11,18,22] and expansion of the *c*-axis dimensions [5], and these lattice expansions/contractions appear to vary linearly with lattice carbonate content [52]. Our simulations show the same trends in lattice parameters as experiment, as is shown in Table 3. The small increase in the *a*-dimension upon the incorporation of a carbonate in the channel position is due to its greater bulk compared to a hydroxy group, especially as the carbonate is lined up in the *c*-direction with two of its oxygens above and below the carbon atom, but with the third oxygen atom rotating in the *a*/*b* plane, which leads to an expansion in these directions.

The changes in *a*- and *b*-parameters for the different isolated type-B defects all follow the same trends, although to different degrees. The carbonate group is smaller than a phosphate, hence the contraction in the *a*- and *b*-parameters, when a carbonate is substituted for a phosphate. For the $CO_3$/OH defect, the decrease in the *b*-parameter is much less than the *a*-direction, due to the extra charge compensating $OH^-$ ion incorporated in the lattice. Together the carbonate and OH groups form a rather bulky defect, which distorts the lattice, leading to the unequal modifications of the *a*- and *b*-parameters.

The decrease in lattice parameters for the charge compensating $Na^+$ ion is larger than for $K^+$, which is due to the similar ionic radii of $Na^+$ and the $Ca^{2+}$ ion it replaces. Hence, the decrease in lattice parameters for $Na^+$ is due completely to the smaller carbonate group occupying a phosphate lattice position, whereas for the $K^+$ there will be some expansion of the lattice due to its larger size. However, this increase is still outweighed by the decrease due to the substituting carbonate, but the net effect is smaller.

Finally, in the mixed type-A/B defect we find a decrease in the *a*- and *b*-parameters of the apatite lattice and an increase in the *c*-parameter, which is more than the sum of the isolated type-A and -B defects that it resembles and probably largely due to the crowding of the carbonate group in a single vacancy site in the hydroxy channel. The a- and *b*-parameters have decreased even more than in the type-B defects alone, indicating a greater distortion of the apatite unit cell.

### 3.5. Energetics of ion-exchange from solution

We can use Eqs. (1)–(4) to calculate the formation energies of the individual defect structures. However, although these defect formation energies give us information about the relative stabilities of the many different possible structures for each type of defect, we would have no information about the stabilities of the different defect types with respect to each other. As such, we would not be able to assess which of the range of defects was energetically the most favourable. In order to consider the relative stabilities of the different defect structures and

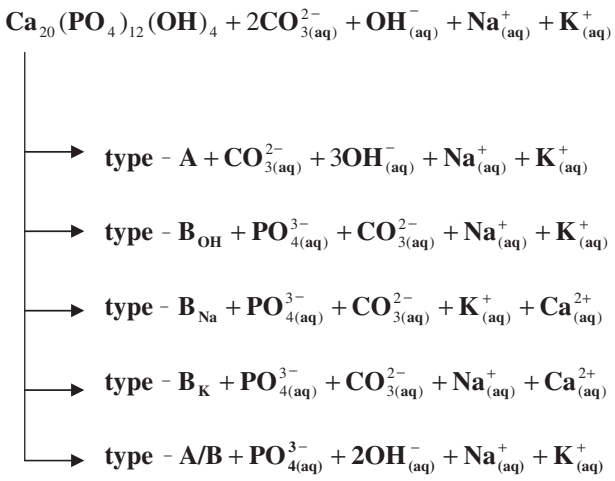


Fig. 7. Reaction schemes of ion-exchange reactions.

Table 4
Calculated lattice energies of hydrated species from molecular dynamics simulations

| Ion | Calculated energy of hydrated ion ($kJ\,mol^{-1}$) |
|---|---|
| $PO^{3-}_{4(aq)}$ | −4698.8 |
| $CO^{2-}_{3(aq)}$ | −4081.3 |
| $OH^-_{(aq)}$ | −723.6 |
| $Na^+_{(aq)}$ | −279.8 |
| $K^+_{(aq)}$ | −183.3 |
| $Ca^{2+}_{(aq)}$ | −1321.8 |

Table 5
Calculated defect formation energies from ion-exchange reactions

| Defect formation energies ($kJ\,mol^{-1}$) | |
|---|---|
| Type-A | −404.0 |
| Type-$B_{OH}$ | −0.7 |
| Type-$B_{Na}$ | −71.1 |
| Type-$B_K$ | −5.6 |
| Type-A/B | −518.7 |

their likelihood of formation, we have designed a series of ion-exchange reactions from solution, which all contain the same reactants, but which have different products according to what defect is formed (Fig. 7). The energies of the various solvated ions, shown in Table 4, were obtained from MD simulations of the ion in a simulation cell filled with 255 water molecules. By calculating the energies of these exchange reactions, we can now directly compare the exchange reactions for each defect with the others to determine their relative order of stability.

Table 5 shows the calculated defect formation energies using the ion exchange reactions from Fig. 7. It is clear from the reaction equations in Fig. 7 and the energies of the aqueous ions in Table 4 that the final energies for the exchange reactions will be due to a combination of factors; firstly there is the energy of the defect lattice itself and, secondly, there is the replacement of lattice ions by hydrated ions from solution. If the hydrated ion has a large negative energy in solution, compared with the lattice ion it is to replace, then ion exchange will be energetically favourable only if the defect structure is of a lower energy than the pure lattice, for example when a large ion is replaced by a smaller one.

As we already discussed above, we see that the $CO_3$/Na type-B defect is more stable than the $CO_3$/K type-B defect, the formation of which is almost energetically neutral. It is clear from Table 4 that the hydrated phosphate ion has a larger energy than the solvated carbonate ion, which thus encourages ion exchange of a lattice phosphate by a carbonate from solution. Similarly, exchange of a lattice calcium for either a hydrated sodium or potassium ion will be energetically favourable. These two exchanges explain why the total exchange reactions and the formation of the type-$B_{Na}$ and -$B_K$ defects is energetically favourable. However, as we can see from Table 4, it is energetically more favourable to exchange an aqueous potassium ion from solution by a lattice calcium ion than it is to replace an aqueous sodium ion (by about $100\,kJ\,mol^{-1}$) and, as all other factors are the same for the formation of these two type-B defects, the added stability of the type-$B_{Na}$ defect compared to the type-$B_K$ therefore must be due to the cation defect structure itself, rather than the energy of the solvated ion which acts in the opposite direction. It is unlikely that the $Na^+$ ion itself will contribute much to the local defect structure as it and the $Ca^{2+}$ ion are of equal size. However, as already discussed above, the ionic radius of the $K^+$ is significantly larger than that of the $Ca^{2+}$ ion, and it is this effect which by elimination of all other factors, leads to the lesser stability of the type-$B_K$ defect in the apatite lattice. We can even estimate this size effect quantitatively by referring again to Tables 4 and 5: the difference in hydration energies of the $K^+$ and $Na^+$ ions of $96.5\,kJ\,mol^{-1}$ together with the difference in their defect formation energies of $65.5\,kJ\,mol^{-1}$ gives an energy of $162\,kJ\,mol^{-1}$, which is the measure of instability of the $K^+$ ion in the lattice compared to the presence of the $Na^+$ ion. The greater affinity of $Na^+$ for the hydroxyapatite lattice compared with $K^+$ is borne out by experimental work of Moens et al. [21] who determined a substitution of approximately 15 mol% $Ca^{2+}$ by $Na^+$ in the hydroxyapatite lattice associated with B-type carbonate defects.

If we now consider the third type-B defect, where the phosphate is replaced by a carbonate and a hydroxy group, we see that the energy of the hydrated phosphate group is smaller (by $106.1\,kJ\,mol^{-1}$) than the sum of the energies of the hydrated carbonate and hydroxy groups and the pure, defect-free structure is hence favoured on the basis of these hydration energies. However, the defect formation energy is approximately zero and the difference in lattice energies between defect-free and defective structures hence balance the difference in hydration energies, indicating that the

defect is stable in the lattice. Although the carbonate group is smaller than the phosphate group and hence should be fairly easy to incorporate at a phosphate site, the presence of a hydroxy group negates the size argument to a certain extent. However, unlike the four oxygen atoms bonded to the phosphorus atom in the phosphate group, the hydroxy group is free to move and rotate independently from the carbonate group, as is clear from the lowest energy defect structure shown in Fig. 4. As such, the defect structure is fairly flexible, leading to its relative stability.

Formation of the type-A defect is obviously energetically very favourable, which cannot be due to the energies of the hydrated ions, as the energy of the two hydroxy groups released into solution is far less than the energy of the carbonate ion taken up into the lattice ($\Delta E = 2634.1\,\mathrm{kJ\,mol^{-1}}$). As such the favourable defect formation energy will be due to the stability of the defect structure itself. Although the carbonate group is larger than a hydroxy group, we have seen from the MD simulations that the carbonate group in fact has a considerable degree of freedom of movement within the hydroxy channel. In fact, as the carbonate replaces two hydroxy groups in the *c*-direction and as the apatite lattice has expanded in the *a*/*b*-directions upon incorporation of the carbonate, its larger size is not really an issue. In addition, as we have seen above, the carbonate with its three oxygen atoms is capable of forming multiple interactions with Ca ions in the lattice, which is not possible to the same extent for the hydroxy groups, as well as retaining the interaction with neighbouring hydroxy groups. As a result of the lattice expansion and these interionic interactions, formation of the A-type defect is energetically very favourable.

It is clear from Table 5 that the combined type-A/B defect is the most favourable reaction product to form from the mixture of reactants. However, the type-A/B defect contains two substitutional carbonate groups and if we consider the energies per substituted carbonate group (i.e. $-259.3\,\mathrm{kJ\,mol^{-1}}/CO_3^{2-}$ on average), the type-A defect is still the most stable and could hence be expected to form first. In fact, the defect formation energy of this mixed type-A/B defect provides us with the means to calculate the process of moving the extra $OH^-$ ion of the type-$B_{OH}$ defect from its location near the substitional carbonate group in the phosphate position to a channel location near the type-A channel carbonate, according to Eq. (5):

$$\text{Type-A} + \text{Type-B}_{OH} \rightarrow \text{Type-A/B}. \quad (5)$$

If we have an apatite lattice where the two defects are present as a carbonate ion replacing two channel hydroxy groups and a carbonate and hydroxy group replacing one phosphate group (i.e. the sum of the type-A and -$B_{OH}$ defects), the defect formation energy is $-404.7\,\mathrm{kJ\,mol^{-1}}$. However, when we move the $OH^-$ ion from its location in the phosphate position to the hydroxy channel, the defect formation energy is $-518.7\,\mathrm{kJ\,mol^{-1}}$, an energy gain of $-114\,\mathrm{kJ\,mol^{-1}}$. Clearly, the hydroxy group prefers to be in the channel position, even with the substitutional channel carbonate group present as well, and the presence of A-type defects thus promotes the formation of type-B defects as well, in agreement with experiment where often combinations of type-A and -B defects are found in the same apatite material [6,7,13,23,24].

## 4. Conclusion

In this study we have employed computer modelling techniques to investigate the uptake and distribution of substitutional carbonate groups in the hydroxyapatite lattice. Our calculations have shown that the A-type defect, where two hydroxy groups are replaced by one carbonate group in the hydroxy channel is the most stable defect structure, but that formation of the B-type defect is also energetically feasible, depending on the charge compensating species, and its formation is also promoted by the presence of A-type defects in the lattice. In addition, it appears both from our calculations and from the experimental literature, that the orientation of the B-type defect may be affected quite strongly by the composition of the apatite material.

Strong evidence for both A- and B-type carbonate defects is provided by a variety of experimental techniques: X-ray diffraction, fourier transform infra-red spectroscopy (FTIR) [15], electron paramagnetic resonance (EPR) and electron-nuclear double resonance (ENDOR) [21], nuclear magnetic resonance (NMR) [7,18] and neutron-scattering [10]. Synthetic and high-temperature apatites often contain A-type defects, especially at low carbonate concentrations [14,17,21,52], or a mixture of both A- and B-type defects in the lattice [14,17,21], but B-type defects appear to prevail in natural bone and, to a lesser degree, in tooth enamel [13,17,53,54]. The occurrence of A-type or mixed A/B-type carbonate defects in synthetic apatites obviously agrees with our calculations, whereas the prevalence of the less energetically favourable B-type carbonate defects on their own in natural bone is probably not as anomalous as it may appear. The structure and stoichiometry of both the synthetic and computer simulated apatites are very carefully controlled and we are therefore confident that we are closely reproducing the experimental material in our calculations. However, natural bone is a composite material, made up of organic material such as collagen [2,53,55] and often containing other calcium phosphate phases, such as octa-calcium phosphate and even amorphous calcium phosphate material [2,12,53]. Even the crystalline apatitic phase in bone contains many defects and impurities and the natural bone material thus only loosely resembles the computer simulated structures. It is therefore possible that we have not sampled lower-energy replacement reactions for the formation of the B-type defects, for example by leaving $Ca^{2+}$ vacancies in the lattice rather than replacing $Ca^{2+}$ by $Na^+$.

One possible scenario for the incorporation of the B-type carbonate defects in the bone apatite is during nucleation

and growth of the material. The apatitic phase is often formed from calcium phosphate precursor phases, such as octa-calcium phosphate which is structurally similar to apatite in some regions and is thought to exist at the surface of the growing bone apatite before crystallising into hydroxyapatite proper [53]. One feature of these precursor phases is the absence of the hydroxy channels and as such, if carbonate is present in the reaction mixture, it would almost certainly replace phosphate groups in the lattice of the growing material, rather than hydroxy groups which are not as yet part of the crystal lattice.

Future work will therefore include further calculations of different defect structures in the hydroxyapatite lattice, including Ca vacancies, interstitial water and other impurity species as well as simulations of the stability of B-type carbonate defects in calcium phosphate precursor phases.

## Acknowledgements

NHdL thanks the Engineering and Physical Sciences Research Council, UK, for an Advanced Research Fellowship and for grant no. GR/S67142/01.

## References

[1] Deer WA, Howie RA, Zussman J. An introduction to the rock-forming minerals. Harlow, UK: Longman; 1992.
[2] Narasaraju TSB, Phebe DE. Some physico-chemical aspects of hydroxylapatite. J Mater Sci 1996;31:1–21.
[3] Ambrosio AMA, Sahota JS, Khan Y, Laurencin CT. A novel amorphous calcium phosphate polymer ceramic for bone repair: 1. Synthesis and characterization. J Biomed Mater Res (Appl Biomater) 2001;58:295–301.
[4] Cho SB, Miyaji F, Kokubo T, Nakanishi K, Soga N, Nakamura T. Apatite formation on silica gel in simulated body fluid: effects of structural modification with solvent-exchange. J Mat Sci—Mat Med 1998;9:279–84.
[5] Baig AA, Fox JL, Young RA, Wang Z, Hsu J, Higuchi WI, Chettry A, Zhuang H, Otsuka M. Relationships among carbonated apatite solubility, crystallite size and microstrain parameters. Calcif Tissue Int 1999;64:437–49.
[6] Yasukawa A, Kandori K, Ishikawa T. TPD-TG-MS study of carbonate calcium hydroxyapatite particles. Calcif Tissue Int 2003; 72:243–50.
[7] Kolodziejski W. Solid-state NMR studies of bone. Top Curr Chem 2004;246:235–70.
[8] Nelson DGA, Featherstone JDB, Duncan JF, Cutress TW. Paracrystalline disorder of biological and synthetic carbonate-substituted apatites. J Dent Res 1982;61:1274–81.
[9] LeGeros RZ, Kijkowska R, Bautista C, LeGeros JP. Synergistic effects of magnesium and carbonate on properties of biological and synthetic apatites. Connect Tissue Res 1995;32:525–31.
[10] Loong CK, Rey C, Kuhn LT, Combes C, Wu Y, Chen SH, Glimcher MJ. Evidence of hydroxyl-ion deficiency in bone apatites: an inelastic neutron-scattering study. Bone 2000;26:599–602.
[11] Elliott JC, Holcomb DW, Young RA. Infrared determination of the degree of substitution of hydroxyl by carbonate ions in human dental enamel. Calcif Tissue Int 1985;37:372–5.
[12] Miller LM, Vairavamurthy V, Chance MR, Mendelsohn R, Paschalis EP, Betts F, Boskey AL. In situ analysis of mineral content and crystallinity in bone using infrared micro-spectroscopy of the $\nu_4$ $PO_4^{3-}$ vibration. Biochim Biophys Acta 2001;1527:11–9.
[13] Morgan EF, Yetkinler DN, Constantz BR, Dauskardt RH. Mechanical properties of carbonated apatite bone mineral substitute: strength, fracture and fatigue behaviour. J Mater Sci: Mater Med 1997;8:559–70.
[14] Suetsugu Y, Takahashi Y, Okamura FP, Tanaka J. Structure analysis of A-type carbonate apatite by a single-crystal X-ray diffraction method. J Solid State Chem 2000;155:292–7.
[15] Fleet ME, Liu X, King PL. Accommodation of the carbonate ion in apatite: An FTIR and X-ray structure study of crystals synthesized at 2–4 GPa. Am Mineral 2004;89:1422–32.
[16] Peeters A, De Maeyer EAP, Van Alsenoy C, Verbeeck RMH. Solids modeled by ab initio crystal-field methods. 12. Structure, orientation and position of A-type carbonate in a hydroxyapatite lattice. J Phys Chem B 1997;101:3995–8.
[17] Vignoles M, Bonel G, Holcomb DW, Young RA. Influence of preparation conditions on the composition of type B carbonated hydroxyapatite and on the localization of the carbonate ions. Calcif Tissue Int 1988;43:33–40.
[18] Kaflak-Hachulska A, Samonson A, Kolodziejski W. $^{1}H$ MAS and $^{1}H$–$^{31}P$ CP/MAS NMR study of human bone mineral. Calcif Tissue Int 2003;73:476–86.
[19] Harries JE, Hasnain SS, Shah JS. EXAFS study of structural disorder in carbonate-containing hydroxyapatites. Calcif Tissue Int 1987;41:346–50.
[20] Kim HM, Kishimoto K, Miyaji F, Kokubo T. Composition and structure of apatite formed on organic polymer in simulated body fluid with a high content of carbonate ion. J Mat Sci: Mater Med 2000;11:421–6.
[21] Moens PD, Callens FJ, Matthys PF, Verbeeck RM. P-31 and H-1 powder ENDOR and molecular-orbital study of a $CO_3^{3-}$ ion in X-irradiated carbonate containing hydroxyapatites. J Chem Soc Faraday Trans 1994;90:2653–62.
[22] Okazaki M, Takahashi J, Kimura H, Aoba T. Crystallinity, solubility and dissolution rate behavior of fluoridated $CO_3$ apatites. J Biomed Mater Res 1982;16:851–60.
[23] Barralet J, Best S, Bonfield W. Carbonate substitution in precipitated hydroxyapatite: an investigation into the effect of reaction temperature and bicarbonate ion concentration. J Biomed Mat Res 1998;41: 79–86.
[24] Moens P, Callens F, Van Doorslaer S, Matthys P. ENDOR study of an $O^-$ ion observed in X-ray-irradiated carbonated hydroxyapatite powders. Phys Rev B 1996;53:5190–7.
[25] Joris SJ, Amberg CH. The nature of deficiency in nonstoichiometric hydroxyapatites. II. Spectroscopic studies of calcium and strontium hydroxyapatites. J Phys Chem 1971;75:3172–8.
[26] Meyer JL, Fowler BO. Lattice defects in nonstoichiometric calcium hydroxylapatites. A Chemical Approach. Inorg Chem 1982;21:3029–35.
[27] Born M, Huang K. In dynamical theory of crystal lattices. Oxford: Oxford University Press; 1954.
[28] Dick BG, Overhauser AW. Theory of the dielectric constants of alkali halide crystals. Phys Rev 1958;112:90–103.
[29] Watson GW, Kelsey ET, deLeeuw NH, Harris DJ, Parker SC. Atomistic simulation of dislocations, surfaces and interfaces in MgO. J Chem Soc Faraday Trans 1996;92:433–8.
[30] Mkhonto D, de Leeuw NH. A computer modelling study of the effect of water on the surface structure and morphology of fluorapatite: introducing a $Ca_{10}(PO_4)_6F_2$ potential model. J Mat Chem 2002;12:2633–42.
[31] Du Z, de Leeuw NH. A combined density functional theory and interatomic potential-based simulation study of the hydration of nano-particulate silicate surfaces. Surf Sci 2004;554:193–210.
[32] de Leeuw NH, Cooper TG. The layering effect of water on the structure of scheelite. Phys Chem Chem Phys 2003;5:433–6.
[33] de Leeuw NH. A computer modeling study of the uptake and segregation of fluoride ions at the hydrated hydroxyapatite (0 0 0 1) surface: introducing $Ca_{10}(PO_4)_6(OH)_2$ potential model. Phys Chem Chem Phys 2004;6:1860–6.

[34] Smith W, Forester TR. DL_POLY_2.0: a general-purpose parallel molecular dynamics simulation package. J Molec Graph 1996;14: 136–41.
[35] Verlet L. Computer experiments on classical fluids. I. Thermodynamical properties of Lennard-Jones molecules. Phys Rev 1967; 159:98.
[36] Nosé S. A unified formulation of the constant temperature molecular-dynamics methods. J Chem Phys 1984;81:511–9.
[37] Hoover WG. Canonical dynamics—equilibrium phase-space distributions. Phys Rev A 1985;31:1695–7.
[38] Pavese A, Catti M, Parker SC, Wall A. Modelling of the thermal dependence of structural and elastic properties of calcite, $CaCO_3$. Phys Chem Miner 1996;23:89–93.
[39] de Leeuw NH, Parker SC. Surface structure and morphology of calcium carbonate polymorphs calcite, aragonite and vaterite: an atomistic approach. J Phys Chem B 1998;102:2914–22.
[40] de Leeuw NH. Molecular dynamics simulations of the growth inhibiting effect of $Fe^{2+}$, $Mg^{2+}$, $Cd^{2+}$ and $Sr^{2+}$ on calciate crystal growth. J Phys Chem B 2002;106:5241–9.
[41] de Leeuw NH, Cooper TG. A computer modeling study of the inhibiting effect of organic adsorbates on calcite crystal growth. Cryst Growth Design 2004;4:123–33.
[42] Purton JA, Allan NL, Blundy JD. Calculated solution energies of heterovalent cations in forsterite and diopside: implications for trace element partitioning. Geochim Cosmochim Acta 1997;61:3927–36.
[43] Schröder KP, Sauer J, Leslie M, Catlow CRA. Bridging hydroxyl-groups in zeolitic catalysts—a computer-simulation of their structure, vibrational properties and acidity in protonated faujasites (H–Y zeolites). Chem Phys Lett 1992;188:320–5.
[44] de Leeuw NH. Local ordering of hydroxy groups in hydroxyapatite. Chem Commun 2001;17:1646–7.
[45] de Leeuw NH. Density functional theory calculations of local ordering of hydroxy groups and fluoride ions in hydroxyapatite. Phys Chem Chem Phys 2002;4:3865–71.
[46] Fleet ME, Liu X. Carbonate apatite type A synthesized at high pressure: new space group (*P3*) and orientation of channel carbonate ion. J Solid State Chem 2003;174:412–7.
[47] Fleet ME, Liu X. Local structure of channel ions in carbonate apatite. Biomaterials 2005;26:7548–54.
[48] Ivanova TI, Frank-Kamenetskaya OV, Koltsov AB, Ugolkov VL. Crystal structure of calcium-deficient carbonated hydroxyapatite. Thermal decomposition. J Solid State Chem 2001;160:340–9.
[49] Wilson RM, Elliott JC, Dowker SEP, Smith RI. Rietveld structure refinement of precipitated carbonate apatite using neutron diffraction data. Biomaterials 2004;25:2205–13.
[50] Lide DR. CRC Hand book of chemistry and physics. Boca Raton, FL: CRC; 2000.
[51] Fleet ME, Liu X. Location of type B carbonate ion in type A–B carbonate apatite synthesized at high pressure. J Solid State Chem 2004;177:3174–82.
[52] Schramm DU, Terra J, Rossi AM, Ellis DE. Configuration of $CO_2^-$ radicals in $\gamma$-irradiated A-type carbonated apatites: theory and experimental EPR and ENDOR studies. Phys Rev B 2000;63 024107, 1–14.
[53] Brown WE, Chow LC. Chemical properties of bone mineral. Annu Rev Mater Sci 1976;6:213–35.
[54] Sadlo J, Matthys P, Vanhaelewyn G, Callens F, Michalik J, Stachowicz W. EPR and ENDOR of radiation-induced $CO_3^{3-}$ radicals in human tooth enamel heated at 400 °C. J Chem Soc Faraday Trans 1998;94:3275–8.
[55] Lawson AC, Czernuszka JT. Collagen-calcium phosphate composites. Proc Instn Mech Eng 1998;212:413–25.